One step production of silver-copper (Agcu) nanoparticles

metals

MDPI

Article

One Step Production of Silver-Copper (AgCu) Nanoparticles

Münevver Köroğlu [1], Burçak Ebin [2], Srecko Stopic [3,*], Sebahattin Gürmen [1] and Bernd Friedrich [3]

[1] Department of Metallurgical & Materials Engineering, Istanbul Technical University, Istanbul 34469, Turkey; koroglu@itu.edu.tr (M.K.); gurmen@itu.edu.tr (S.G.)
[2] Department of Nuclear Chemistry and Industrial Materials Recycling, Chalmers University of Technology, Kemivagen 4, 41296 Gothenburg, Sweden; burcak@chalmers.se
[3] IME Process Metallurgy and Metal Recycling, RWTH Aachen University, 52056 Aachen, Germany; bfriedrich@ime-aachen.de
* Correspondence: sstopic@ime-aachen.de; Tel.: +49-176-7826-1674

Abstract: AgCu nanoparticles were prepared through hydrogen-reduction-assisted Ultrasonic Spray Pyrolysis (USP) and the Hydrogen Reduction (HR) method. The changes in the morphology and crystal structure of nanoparticles were studied using different concentrated precursors. The structure and morphology of the mixed crystalline particles were characterized through X-ray diffraction analysis (XRD), scanning electron microscopy (FEG-SEM), transmission electron microscopy (TEM) and Energy-dispersive X-ray spectroscopy (EDS). The average particle size decreased from 364 nm to 224 nm by reducing the initial solution concentration from 0.05 M to 0.4 M. These results indicate that the increase in concentration also increases the grain size. Antibacterial properties of nanoparticles against Escherichia coli were investigated. The obtained results indicate that produced particles show antibacterial activity (100%). The AgCu nanoparticles have the usage potential in different areas of the industry.

Keywords: silver; copper; nanoparticles; ultrasonic spray pyrolysis; antibacterial

Citation: Köroğlu, M.; Ebin, B.; Stopic, S.; Gürmen, S.; Friedrich, B. One Step Production of Silver-Copper (AgCu) Nanoparticles. *Metals* **2021**, *11*, 1466. https://doi.org/10.3390/met11091466

Academic Editor: Leonid M. Kustov

Received: 7 August 2021
Accepted: 14 September 2021
Published: 16 September 2021

Highlights

AgCu nanoparticles have been produced in one step by ultrasonic spray pyrolysis.
AgCu particle size was controlled by changing the concentration of the solution.
AgCu nanosized particles exhibit improved antibacterial activity.

1. Introduction

In recent years, there has been increasing interest in bimetallic nanoparticles because of their potential applications to magnetism, catalysis and optics. These nanoparticles are often called nanoalloys [1]. Bimetallic nanoparticles, either as alloys or as core–shell structures, exhibit unique electronic, optical and catalytic properties compared to monometallic nanoparticles [2,3]. Several bimetallic nanoparticles have been recommended for use in a catalytic system [4–6]. A series of bimetallic catalysts, such as Cu-Au, Cu-Pd, Cu-In and Cu-Sn, have been introduced to exhibit improved surface activities toward CO. Cu-Pt alloy or Cu-modified Pt electrocatalysts still could show the capability of Cu to reduce CO_2 into hydrocarbon products [7].

Although a lot of work has been done on the preparation of noble metal alloys, there are only a few reports on bimetallic particles of copper, especially with silver. Lattice constants of Ag and Cu are 0.409 nm and 0.361 nm, respectively, and this large difference in the lattice constants of Cu and Ag makes the preparation of their alloy difficult. Additionally, it is difficult to control the simultaneous reduction of Cu and Ag because of the difference in redox potential, and the instability of Cu in an aqueous medium is an added difficulty [2]. The fact that copper (Cu) is an important metal used in modern technologies increases its attention [8]. Nanospheric Cu particles are more attractive than other metals because of their advantages, such as being cheap, easy to find and their wide range of uses [8,9]. Based

on these advantages, Cu nanoparticles, capacitor material, catalyst, conductive coating, ink-jet printing technology, conductive paste, insulating material, oil additive and sintering additives can be used [10,11]. In particular, Cu has gained more interest because of its capability to reduce CO_2 into hydrocarbon fuels [12]. It has long been known that silver (Ag) is a very strong antibacterial material in both metallic form and compound forms, and its inhibitory effect on bacteria has been studied by many researchers [13–15]. Ag nanoparticles are a gold standard bacteriostatic agent [16]. Ag is known to be used in antibacterial applications since ancient times, and Ag nanoparticles are often preferred in biosensor applications [17]. Ag nanoparticles play an important role in increasing the sensitivity of biosensors because of their ability to accelerate the transfer of electrons [16–19]. The seriousness of problems with energy supplies and environmental pollution is creating greater interest in fuel cells and lithium batteries [20–22]. Fuel cells produce electricity by electrochemically converting hydrogen and oxygen into water, and noble metals, such as Pt, are used as a catalyst for the oxygen reduction reaction. However, the high cost of Pt has sparked a search for a Pt substitute or new ways of reducing the quantity of Pt required. AgCu bimetallic nanoparticles have proper adsorption strength and become a good catalyst for the oxygen reduction reaction. Moreover, Ag and Cu are considerably less expensive than Pt or Pd [6].

Various methods have been proposed to synthesize metallic nanoparticles, including wet chemical reduction, electrochemical, laser ablation and solution combustion [23–27]. Among them, the ultrasonic spray pyrolysis (USP) technique has been rarely used for this purpose. The USP technique was preferred for its low cost and especially for its simplicity for fabricating oxides with good qualities [28]. The wet chemical synthesis is based on the reduction of metals salts by a reducing agent. It consists of many steps to obtain products, and controlling the process is challenging compared to the USP method. Strong reducing agents are necessary for producing metallic nanoparticles, such as sodium borohydride [29], hydrazine [30] and sodium hypophosphite [31]. USP is a process in which solid particles are produced by evaporation, drying and thermal decomposition/reduction processes in a controlled atmosphere, starting from droplets obtained from ultrasonic frequency from metal salt precursors. Single-step and atmospheric pressure droplet to particle conversion and particle collection processes in USP results in spherical, needle-like, plate, flower-like, diagonal and micro- or nanosized metal, as well as oxide, ceramic, carbon-based or nanocomposite-agglomerated materials with a narrow size distribution [32–35].

In this study, we aimed to produce nanoalloy particles, which can be used in energy supplies (fuel cells, lithium batteries) and antibacterial products. Since there is no previous study that has been reported on the synthesis of the AgCu nanoalloy by the USP-HR method, the antibacterial particles were prepared with the one-step method with a controlled Ag content and particle morphology, which is the original aspect presented in this study. In comparison to the previous synthesis of single nanosized particles of copper and silver, this USP synthesis from mixed precursors will offer the improved characteristics of the final AgCu particles [36–40].

2. Experimental

AgCu nanosized particles were synthesized using the aqueous solution of silver nitrate ($AgNO_3$) and copper nitrate ($CuNO_3)_2.3H_2O$) under 1 L/min H_2 flow rate at an 800 °C reduction temperature. The nitrate salts (all from Merck, Darmstadt, Germany) were dissolved in deionized water and stirred with a magnetic stirrer for 30 min. The metal concentration in the precursor was between 0.05 mol/L and 0.4 mol/L. The precursor solution was atomized using an ultrasonic atomizer with a resonant frequency of 1.3 MHz (RBI-Instrumentation, Meylan, France). The reduction of aerosol droplets occurred at 800 °C in the electrically heated furnace with the heating zone of 0.25 m and the diameter of the quartz tube of 0.02 m (Nabertherm, Germany). The details of the experimental parameters for the synthesis of AgCu nanosized particles are given in Table 1.

Table 1. Experimental parameters.

$AgNO_3$ (mol/L)	$Cu(NO_3)_2$ (mol/L)	Temperature (°C)	H_2 Flow Rate (L/min)	N_2 Flow Rate (L/min)	Ultrasonic Frequency (MHz)
0.05	0.05	800	1.0	0.5	1.3
0.1	0.1	800	1.0	0.5	1.3
0.2	0.2	800	1.0	0.5	1.3
0.4	0.4	800	1.0	0.5	1.3

X-ray diffraction patterns were obtained for the crystal structure determination of alloy particles by the Philips-1700 X-ray diffractometer (Philips, Eindhoven, The Netherlands) employing Cu-Kα radiation. The chemical compositions of particles were analyzed by energy dispersive spectroscopy (EDS). The particle size and morphology of the samples were investigated by field emission scanning electron microscopy (FEG-SEM, JEOL JSM 700F, Tokyo, Japan) and transmission electron microscopy (FEI Tecnai G^2F20 S-TWIN-TEM, Hillsboro, OR, USA). The temperature behavior of silver nitrate salt and copper nitrate salts was investigated by using a differential scanning calorimeter and thermal gravimetry (DSC-TG SDT Q600, TA Instrument, New Castle, DE, USA). Moreover, the antibacterial activities of AgCu nanosized particles were evaluated according to the American Society for Testing and Materials (ASTM) E 2149-01 standard test method.

3. Results and Discussion

3.1. Thermodynamic Analysis of Ag and Cu Nitrate Salts

In order to understand the reaction mechanism in the production of nanosized AgCu alloy particles with USP and HR, the breakdown of the Ag and Cu nitrate salts was investigated using thermochemical analysis. For this purpose, the thermal behavior of the Ag and Cu nitrate solutions were investigated, respectively, then the free energy changes of the nitrate salts in the nitrogen and hydrogen atmosphere under the heat dissolution/reduction reactions were investigated using the enthalpy (H), entropy (S) and heat capacity (C) HSC (Outotec, Espoo, Finland) program. The thermal behavior of the nitrate salts used as starting material in experimental studies was carried out by using Differential Scanning Calorimeter-Thermal Gravimetry (DSC-TG), (TA Instrument, New Castle, DE, USA) between the room temperature and 1000 °C using a heating rate of 10 °C/min in a nitrogen atmosphere. Figures 1 and 2 show the thermal behavior of the $AgNO_3$ and $Cu(NO_3)_2.3H_2O$ salts, respectively.

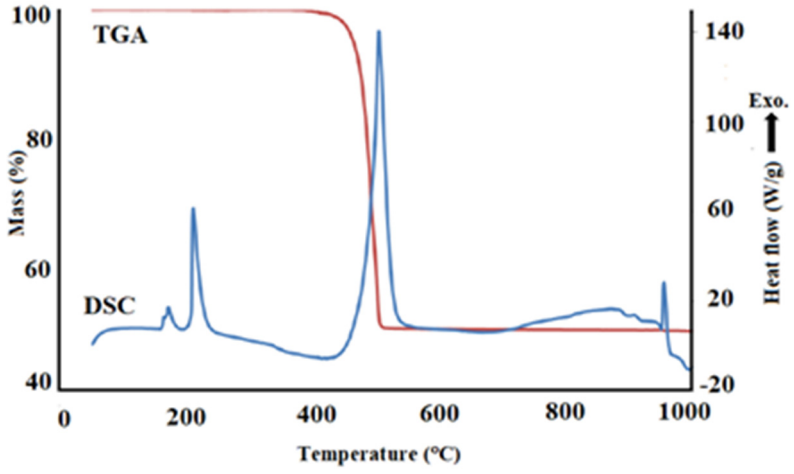

Figure 1. DSC-TGA analysis of $AgNO_3$ salt.

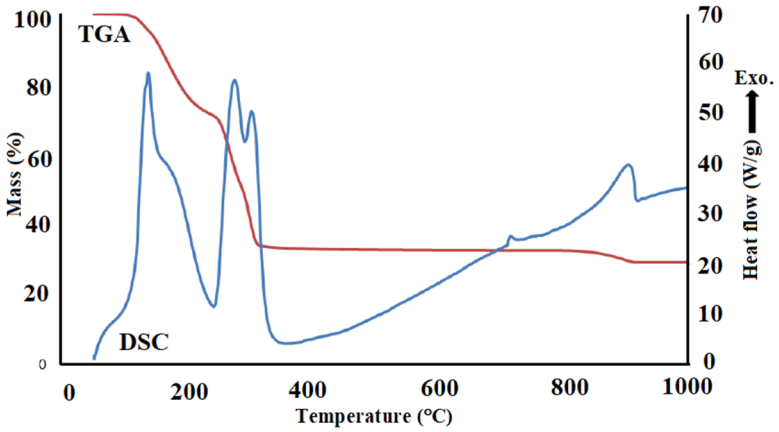

Figure 2. DSC-TGA analysis of $(CuNO_3)_2.3H_2O$) salt.

The expected reaction of the thermal decomposition ware proposed below with Equations (1) and (2):

$$2AgNO_3 = 2Ag + 2NO_2(g) + O_2(g) \quad (1)$$

$$2Cu(NO_3)_2 = 2CuO + 4NO_2(g) + O_2(g) \quad (2)$$

The DSC curve shown in Figure 1 gives a peak indicating that there is an endothermic reaction at a temperature of about 200 °C, while the TG curve indicates some loss of mass at this temperature. The loss of this mass is due to the small amount of crystal water present in the $AgNO_3$ salt. The TG curve indicates a significant loss of mass (about 40%) in the structure around 400 °C, and this mass loss continues to a temperature of 500 °C. After 500 °C, it is observed that there is no mass loss in the structure, and the structure maintains its stability. Considering this and the endothermic reaction peak shown by the DSC curve at the same temperature, it can be said that the $AgNO_3$ salt of this mass loss is subjected to thermal breakdown and the NO_2 gas is away from the structure. The stable structure resulting from this thermal decomposition (after 500 °C) is silver and indicates the melting point of endothermic peak silver at about 950 °C.

The DSC curve shown in Figure 2 shows that there is a mass loss of up to about 250 °C. This mass loss is caused by the removal of the crystal water in the $Cu(NO_3)_2$ salt. The DSC curve seen in the temperature range of this mass loss gives a peak indicating the endothermic reaction. The TG curve indicates a significant loss of mass (approximately 50%) in the structure around 250 °C, and this mass loss continues to a temperature of about 310 °C. After 310 °C, it is observed that there is no mass loss in the structure, and the structure maintains its stability. Considering this and the endothermic reaction peak of the DSC curve at the same temperature, it can be said that this mass loss is caused by the thermal breakdown of $Cu(NO_3)_2$ salt. The stable structure resulting from this thermal decomposition (after 310 °C) is Cu and indicates the melting point of the endothermic peak copper formed at about 880 °C.

In particle production by the USP-HR method, the hydrogenation temperature of the aerosols obtained by atomizing the high purity metal salt is of great importance. For this purpose, the HSC program was used in the investigation of nitrogen and hydrogen gases and thermal decomposition thermodynamics of $AgNO_3$ and $Cu(NO_3)_2$ salts, which we used in our experiments.

Figure 3 shows the graph of the temperature-free energy change obtained by the FactSage program (FactSage, Montreal, QC, Canada and Aachen, Germany) for decomposition of $AgNO_3$ and $Cu(NO_3)_2$. The thermodynamic reaction for hydrogen reduction of $AgNO_3$ and $Cu(NO_3)_2$ can be described as in Equations (3) and (4).

$$AgNO_3 + H_2 = Ag + NO_2(g) + H_2O(g) \quad (3)$$

$$Cu(NO_3)_2 + 2H_2(g) \rightarrow Cu + 2NO_2(g) + 2H_2O \quad (4)$$

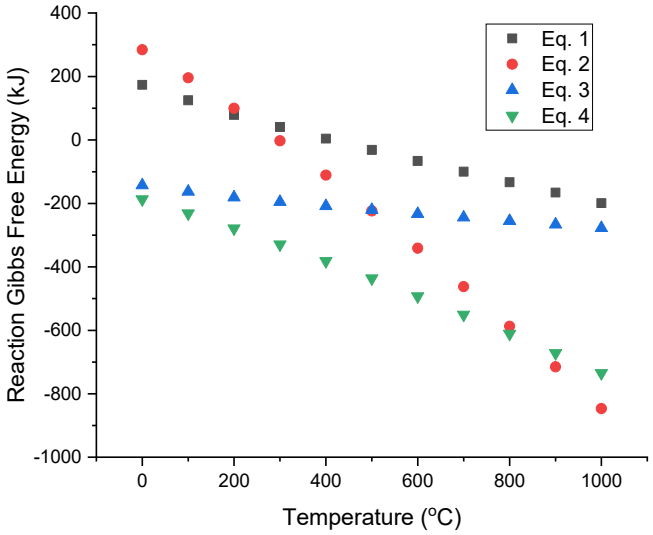

Figure 3. The change of the Gibbs Free Energy value with temperature in the reaction of the $AgNO_3$ salt with hydrogen and nitrogen.

As seen from Figure 3, the reduction of $AgNO_3$ salt with hydrogen is thermodynamically possible at room temperature, where Gibbs free energy is negative, and a decrease in free energy is observed with increasing temperature. In the analysis for the thermal decomposition of $AgNO_3$ in a nitrogen atmosphere, it is seen that the Gibbs free energy change of the reaction remained in the positive zone at low temperatures and decreased with increasing temperature. It is also seen that the thermal decomposition reaction in the nitrogen atmosphere of $AgNO_3$ will begin to occur at 420 °C, where the thermodynamically Gibbs free energy change passes to the negative region. The reduction of $Cu(NO_3)_2$ salt by hydrogen is thermodynamically possible even at 0 °C, where Gibbs free energy is negative. It is also seen that the thermal decomposition reaction in the nitrogen atmosphere of $Cu(NO_3)_2$ begins to occur at 390 °C, where the thermodynamically Gibbs free energy exchange passes to the negative region Equations (1)–(4) and Figure 3 proved that silver and copper could be formed through the hydrogen reduction of silver and copper nitrates.

3.2. Structural Characterization of AgCu Particles

X-ray diffraction patterns of the AgCu alloy nanoparticles produced at an 800 °C reduction temperature using the solutions with different concentrations are given in Figure 4.

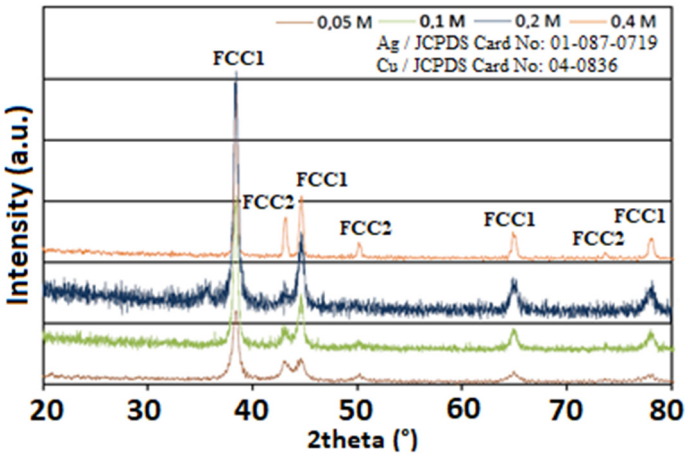

Figure 4. XRD patterns of AgCu nanoparticles (800 °C, 1.0 L/min H_2 flow rate and frequency of 1.3 MHz).

In Figure 4, the peaks at 38°, 44°, 64° and 77° according to 2θ values are assigned to the (111), (200), (220) and (311) reflection lines, and it confirms the formation of a face-centered cubic structure of Ag (JCPDS Card No: 01-087-0719). The face-centered cubic Cu phase at 2θ = 43°, 50° and 74° coincide with (111), (200) and (220) (JCPDS Card No: 04-0836). According to the XRD results, the alloy consisted of FCC1 (α) and FCC2 (β). The diffraction peaks for the stable Ag-rich (α) and Cu-rich (β) phase were observed in Figure 5. In addition, Cu_2O nanoparticles phases were found in the cubic structure at 36° in 2θ values (111) at only a 0.2 M concentration. When the initial solution concentration decreases, the peaks' expansion and the peak's intensity decrease, which can be explained by the decrease in crystalline and particle size. In addition, crystallite sizes were calculated using the Scherrer Equation (5) from the diffraction pattern of the X-ray diffractogram in Figure 5 (see Figure 6).

$$D = \frac{K * \lambda}{B * \cos\theta} \quad (5)$$

where D is the average crystalline size, B is the broadening of the diffraction line measured at half of the maximum intensity, λ is the wavelength (Cu-Kα = 1.541874 Å), θ is the Bragg angle for a given diffraction, and K is a constant, which is a value ranging from 0.85 to 0.9 for powders. Figure 5 shows the average crystalline size of nanosized particles depending on the concentration of the precursor.

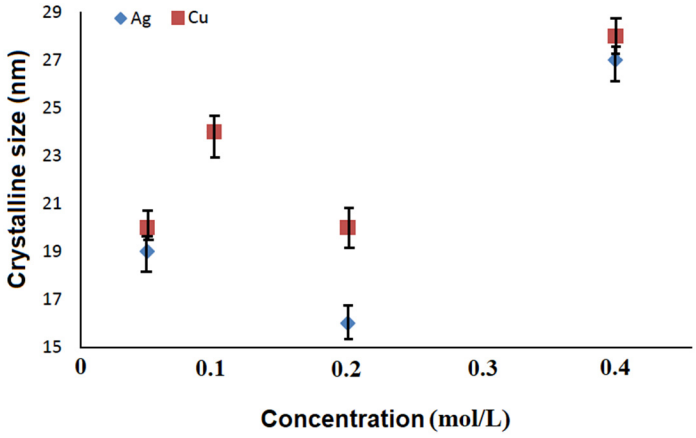

Figure 5. Relationship between concentration and crystalline size (800 °C, 1.0 L/min H_2 flow rate and 1.3 MHz).

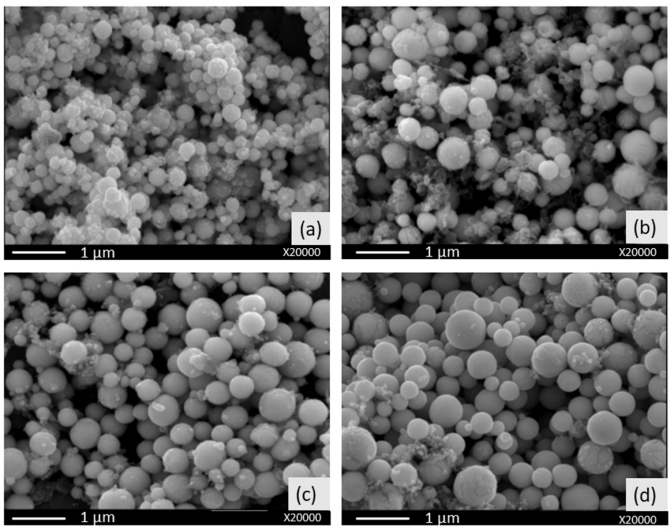

Figure 6. SEM analyses of AgCu nanosized particles, (**a**) 0.05 mol/L, (**b**) 0.1 mol/L, (**c**) 0.2 mol/L and (**d**) 0.4 mol/L.

Figure 5 shows the crystalline size calculated using the Scherrer Equation of the nanoparticles produced from the initial solutions with different concentrations, respectively, from 16 nm to 26 nm for silver and from 20 nm to 28 nm for copper. The nanosized particles obtained using 0.2 M solution exhibit the lowest crystallite size.

3.3. Morphological Characterization of AgCu Nanocomposite Particles

SEM images of the particles obtained by increasing solution concentrations (0.05, 0.1, 0.2 and 0.4 mol/L) at 800 °C are given in Figure 6. All samples exhibit spherical shape morphology and almost smooth surfaces. With the reduction of the solution concentration, it is seen that particles that have a finer particle size and generally a narrower particle size distribution are produced. It was observed that large-grained particles together with very fine grains were present in samples produced from solutions with different concentrations. Furthermore, these produced particles show a tendency to cluster. Growing silver-copper nanoparticles showed a tendency to cluster more with a decrease in concentration. The differences in the agglomeration of the particles produced in the environment where all the conditions except the concentration are the same are explained by the surface area and activity of the particles.

EDS analyses of the nanosized particles are given in Table 2. The presence of Ag and Cu was affirmed by EDS analysis. Any possible impurities, such as nitrogen due to undecomposed reactants, were not detected in the EDS spectrums. However, as a result of EDS analysis of the solution with a concentration of 0.05 M, the presence of oxygen here comes from the possible oxide structure in the sample preparation and is not seen as an impurity in the produced particles.

Table 2. EDS results of AgCu nanoparticles produced at different concentrations at 800 °C.

Concentration (mol/L)	Element (%)		
	Ag	Cu	O
0.05	32.2	46.4	21.4
0.1	48.1	51.9	-
0.2	52.1	47.9	-
0.4	49.1	50.9	-

In order to measure the sizes of particles obtained from the initial solutions of different concentrations, the mean particle sizes were calculated by measuring the dimensions of the particles seen on the SEM images with the help of the ImageJ program (NIH, Maryland, USA) (Figure 7).

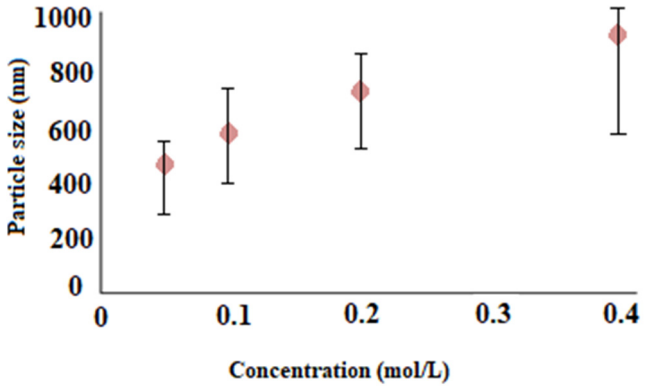

Figure 7. Variation in particle size depending on the initial concentration (800 °C, 1.0 L/min H_2 flow and 1.3 MHz).

When the particle size obtained from 0.05 M silver nitrate-copper nitrate was approximately 224 nm in size, the particles were grown with increasing concentrations, and

particles the size of 364 nm were formed in the 0.4 M concentration. TEM analyses of AgCu nanoparticles produced from silver nitrate and copper nitrate starting solutions with 0.05 M–0.4 M concentrations by the USP-HR technique were performed using the FEI Tecnai G2 F20 S—TWIN 200 kV STEM/TEM device. Particles stored in ethanol were kept in the ultrasonic homogenizer, and the possible agglomerations were removed from the structure. Then, it was covered with copper grids by the immersion method. The results of these characterization studies are given in Figure 8.

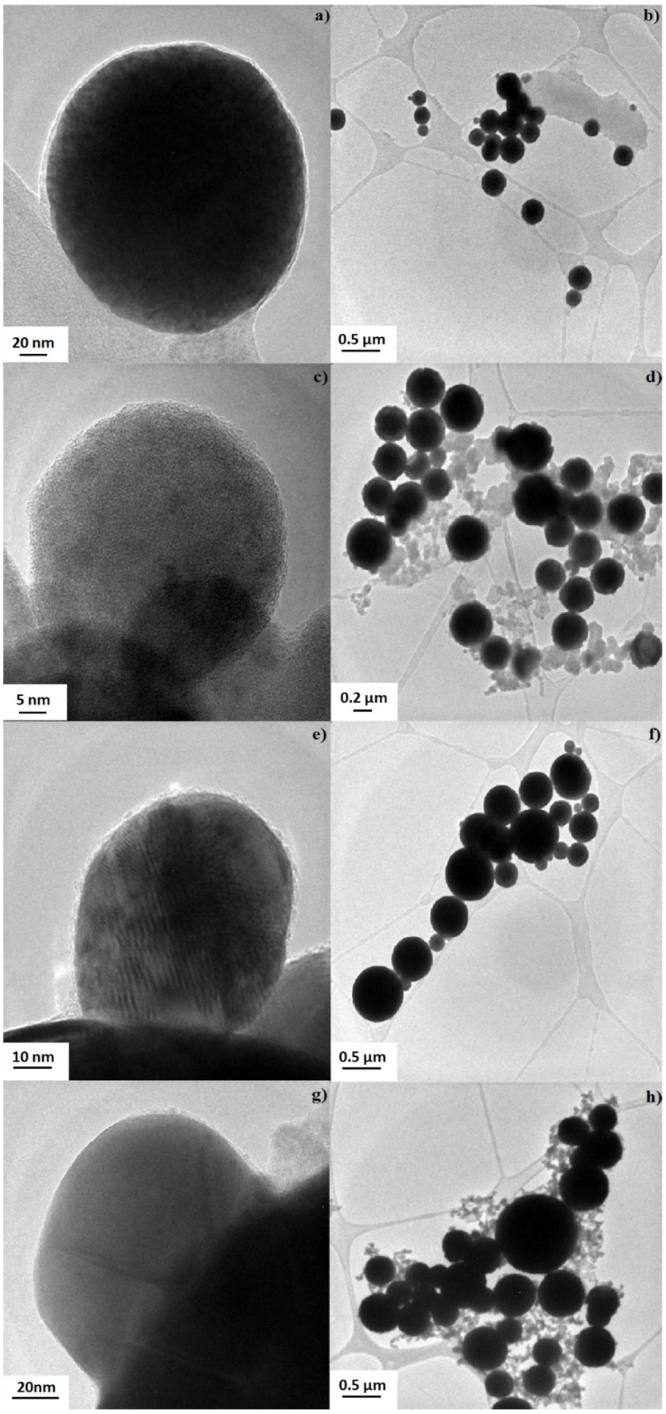

Figure 8. TEM images of AgCu nanosized particles, (**a**,**b**) 0.05 mol/L (**c**,**d**) 0.1 mol/L (**e**,**f**) 0.2 mol/L and (**g**,**h**) 0.4 mol/L.

When Figure 8 is examined, primary particles with a particle size less than 100 nm from the TEM images have been clearly identified (Figure 8a,c,e,g). In addition, secondary particles (≥100 nm) formed by the incorporation of primary particles are clearly seen (Figure 8b,d,f,h). It was determined that the hollow structure was replaced by the dense particle due to sintering at a high temperature.

3.4. Antibacterial Properties of AgCu Nanosized Particles

The measurement of antibacterial activity was made with the AgCu alloy nanoparticles shown in Table 1. The antibacterial activity of the nanosized particles defined in Table 1 was assessed against E. coli (gram-negative) bacteria (American Type Culture Collection (ATCC) 35218) via planting the bacteria in the agar medium according to the American Society for Testing and Materials (ASTM) E 2149-01 standard under dynamic contact conditions. The measurement was made after incubation at 37 °C for 24 h. This test standard is suitable for particles that do not have migrations property. The antibacterial activity of these particles against E. coli bacteria was given in Table 3.

Table 3. The value of antibacterial activity of the nanosized particles against Escherichia coli bacteria after 24 h.

The Sample of Specimen	Bacterial Reduction (%)
Untreated reference sample	+140.00
0.05 mol/L	−100.00
0.1 mol/L	−100.00
0.2 mol/L	−100.00
0.4 mol/L	−100.00

As shown in Table 3, the improved antibacterial (ASTM E 2149-01) properties of AgCu nanoparticles were observed via a decrease in bacterial reduction (approx. 100%)

4. Conclusions

AgCu nanoparticles were successfully synthesized via the hydrogen-reduction-assisted ultrasonic spray pyrolysis method in one step at 800 °C using an aqueous solution of silver/copper nitrates as a precursor. The USP-HR method was used for the production of AgCu nanoparticles in the desired size and morphology by using nitrogen as the inert gas and hydrogen as the carrier/reducing gas. The effects of various precursor concentrations on the morphology and crystal structure of the AgCu nanoparticles were investigated. The average particle size decreased from 364 nm to 224 nm by reducing the initial solution concentration from 0.4 mol/L to 0.05 mol/L. The size range of the AgCu nanoparticles produced in experimental studies is 20 nm–100 nm for the solution where the concentration is 0.05 mol/L, 100–450 nm for 0.1 mol/L, 180–1100 nm for 0.2 mol/L and 50–1050 nm for 4 mol/L. These results indicate that the increase in concentration also increases the grain size. In XRD analysis, silver and copper particles were determined to be cubic structures. The particle crystalline sizes calculated for the concentrations of 0.05 mol/L, 0.1 mol/L, 0.2 mol/L and 0.4 mol/L according to the Scherrer equation, respectively, for silver, 19.92 nm, 24.3 nm, 15.91 nm and 27 nm, and for copper, 20.84 nm, 24.05 nm, 20.4 nm and 28.7 nm for 34 nm. In the TEM images of nanosized AgCu particles, primary particles of smaller than 100 nm and larger secondary particles were observed. Furthermore, the elimination of 100% bacteria was achieved by all synthesized AgCu nanoparticles. Improved antibacterial (ASTM E 2149-01) properties of AgCu nanoparticles demonstrated that these nanoparticles could be used as antibacterial agents in various areas.

Author Contributions: Conceptualization, M.K., B.E. and S.S.; funding acquisition, S.G.; investigation, M.K. and B.E.; methodology, M.K. and S.G.; supervision, S.G. and B.F.; writing—original draft, M.K., S.G. and S.S. All authors have read and agreed to the published version of the manuscript.

Funding: This research received no external funding.

Institutional Review Board Statement: Not applicable.

Informed Consent Statement: Not applicable.

Data Availability Statement: Not applicable.

Acknowledgments: Authors thank Gultekin Goller, Onur Balci, Ikbal Isik and Technician Huseyin Sezer for SEM, TEM and XRD characterizations and for the antibacterial studies.

Conflicts of Interest: The authors declare no conflict of interest.

References

1. Laasonen, K.; Panizon, E.; Bochicchio, D.; Ferrando, R. Competition between Icosahedral Motifs in AgCu, AgNi, and AgCo Nanoalloys: A Combined Atomistic−DFT Study. *J. Phys. Chem. C* **2013**, *117*, 26405–26413. [CrossRef]
2. Valodkar, M.; Modi, S.; Pal, A.; Thakore, S. Synthesis and anti-bacterial activity of Cu, Ag and Cu–Ag alloy nanoparticles: A green approach. *Mater. Res. Bull.* **2011**, *46*, 384–389. [CrossRef]
3. Jabbareh, M.A.; Monji, F. Thermodynamic modeling of Ag-Cu nanoalloy phase diagram. *Calphad* **2018**, *60*, 208–213. [CrossRef]
4. Khan, N.A.; Uhl, A.; Shaikhutdinov, S.; Freund, H.J. Alumina supported model Pd–Ag catalysts: A combined STM, XPS, TPD and IRAS study. *Surf. Sci.* **2006**, *600*, 1849–1853. [CrossRef]
5. Gao, Y.; Shao, N.; Bulusu, S.; Zeng, X.C. Effective CO Oxidation on Endohedral Gold-Cage Nanoclusters. *J. Phys. Chem. C* **2008**, *112*, 8234–8238. [CrossRef]
6. Shin, K.; Kim, D.H.; Yeo, S.C.; Lee, H.M. Structural stability of AgCu bimetallic nanoparticles and their application as a catalyst: A DFT study. *Catal. Today* **2012**, *185*, 94–98. [CrossRef]
7. Chang, Z.; Huo, S.; Zhang, W.; Fang, J.; Wang, H. The Tunable and Highly Selective Reduction Products on Ag@Cu Bimetallic Catalysts toward CO_2 Electrochemical Reduction Reaction. *J. Phys. Chem. C* **2017**, *121*, 11368–11379. [CrossRef]
8. Ciacci, L.; Vassura, I.; Passarini, F. Urban Mines of Copper: Size and Potential for Recycling in the EU. *Resources* **2017**, *6*, 6. [CrossRef]
9. Shahcheraghi, S.H.; Schaffie, M.; Ranjbar, M. Development of an electrochemical process for production of nano-copper oxides: Agglomeration kinetics modeling. *Ultrason. Sonochem.* **2018**, *44*, 162–170. [CrossRef]
10. Zhu, W.; Zhang, L.; Yang, P.; Chang, X.; Dong, H.; Li, A.; Hu, C.; Huang, Z.; Zhao, Z.J.; Gong, J. Morphological and Compositional Design of Pd-Cu Bimetallic Nanocatalysts with Controllable Product Selectivity toward CO2 Electroreduction. *Nano-Micro Small* **2018**, *14*, 1703314. [CrossRef]
11. Pajor-Swierzy, A.; Farraj, Y.; Kamyshny, A.; Magdassi, S. Effect of carboxylic acids on conductivity of metallic films formed by inks based on copper@silver core-shell particles. *Colloids Surf. A* **2017**, *522*, 320–327. [CrossRef]
12. Costentin, C.; Robert, M.; Saveant, J.M. Catalysis of the Electrochemical Reduction of Carbon Dioxide. *Chem. Soc. Rev.* **2013**, *42*, 2423–2436. [CrossRef]
13. Kawashita, M.; Tsuneyama, S.; Miyaji, F.; Kokubo, T.; Kozuka, H.; Yamamoto, K. Antibacterial silver-containing silica glass prepared by sol-gel method. *Biomaterialia* **2000**, *21*, 393–398. [CrossRef]
14. Qin, D.; Yang, G.; Wang, Y.; Zhou, Y.; Zhang, L. Green synthesis of biocompatible trypsin-conjugated Ag nanocomposite with antibacterial activity. *Appl. Surf. Sci.* **2019**, *469*, 528–536. [CrossRef]
15. Sirelkhatim, A.; Mahmud, S.; Seeni, A.; Kaus, N.H.; Ann, L.C.; Bakhori, S.K.; Hasan, H.; Mohamad, D. Review on zinc oxide nanoparticles: Antibacterial activity and toxicity mechanism. *Nano-Micro Lett.* **2015**, *7*, 219–242. [CrossRef]
16. Hong, H.; Cao, G.; Qu, J.; Deng, Y.; Tang, J. Antibacterial activity of Cu2O and Ag co-modified rice grains-like ZnO nanocomposites. *J. Mater. Sci. Technol.* **2018**, *34*, 2359–2367. [CrossRef]
17. Ebrahiminezhad, A.; Raee, M.; Manafi, Z.; Sotoodeh Jahromi, A.; Ghasemi, Y. Ancient and Novel Forms of Silver in Medicine and Biomedicine. *J. Adv. Med. Sci. Appl. Technol.* **2016**, *2*, 122–128. [CrossRef]
18. Ren, X.; Mena, X.; Chen, D.; Tang, F.; Jiao, J. Using silver nanoparticle to enhance current response of biosensor. *Biosens. Bioelectron.* **2005**, *21*, 433–437. [CrossRef]
19. Zuo, F.; Zhang, C.; Zhang, H.; Tan, X.; Chen, S.; Yuan, R.A. solid-state electrochemiluminescence biosensor for Con A detection based on CeO2@Ag nanoparticles modified graphene quantum dots as signal probe. *Electrochim. Acta* **2019**, *294*, 76–83. [CrossRef]
20. Amiri, A.; Tang, S.; Steinberger-Wilckens, R.; Tade, M.O. Evaluation of fuel diversity in Solid Oxide Fuel Cell system. *Int. J. Hydrogen Energy* **2018**, *43*, 27. [CrossRef]
21. Nitta, N.; Wu, F.; Tae Lee, J.; Yushin, G. Li-ion battery materials: Present and future. *Mater. Today* **2015**, *18*, 252–264. [CrossRef]
22. Zubi, G.; Dufo-Lopez, R.; Carvalho, M.; Pasaoglu, P. The lithium-ion battery: State of the art and future perspective. *Renew. Sustain. Energy Rev.* **2018**, *89*, 292–308. [CrossRef]
23. Simakin, A.V.; Voronov, V.V.; Shafeev, G.A.; Brayner, R.; Bozon-Verduraz, F. Nanodisks of Au and Ag produced by laser ablation in liquid environment. *Chem. Phys. Lett.* **2001**, *348*, 182–186. [CrossRef]
24. Chen, Y.H.; Yeh, C.S. Laser ablation method: Use of surfactants to form the dispersed Ag nanoparticles. *Colloids Surf. A* **2002**, *197*, 133–139. [CrossRef]
25. Sharma, P.; Lotey, G.S.; Singh, S. Solution-combustion: The versatile route to synthesize silver nanoparticles. *J. Nanopart. Res.* **2011**, *13*, 2553–2561. [CrossRef]

26. Yin, B.; Ma, H.; Wang, S.; Chen, S. Electrochemical synthesis of silver nanoparticles under protection of poly(N-vinylpyrrolidone). *J. Phys. Chem. B* **2003**, *107*, 8898–8904. [CrossRef]
27. Ishizaki, T.; Watanabe, R. A New One-Pot Method for the Synthesis of Cu Nanoparticles for Low Temperature Bonding. *J. Mater. Chem.* **2012**, *22*, 25198–25206. [CrossRef]
28. Ouhaibi, A.; Ghamnia, M.; Dahamni, A.; Heresanu, V.; Fauquet, C.; Tonneau, D. The effect of strontium doping on structural and morphological properties of ZnO nanofilms synthesized by ultrasonic spray pyrolysis method. *J. Sci. Adv. Mater. Devices* **2018**, *3*, 29–36. [CrossRef]
29. Qiu, S.; Dong, J.; Chen, G. Preparation of Cu nanoparticle from water-in-oil microemulsions. *J. Colloid Interface Sci.* **1999**, *216*, 230. [CrossRef]
30. Wu, S.H.; Chen, D.H. Synthesis of high-concentration Cu nanoparticles in aqueous CTAB solutions. *J. Colloid Interface Sci.* **2004**, *273*, 165. [CrossRef]
31. Zhu, H.T.; Zhang, C.Y.; Yin, Y.S. Rapid synthesis of copper nanoparticles by sodium hypophosphite reduction in ethylene glycol under microwave irradation. *J. Cryst. Growth* **2004**, *270*, 722. [CrossRef]
32. Stopic, S.; Schroeder, M.; Weirich, T.; Friedrich, B. Synthesis of TiO_2 Core/RuO_2 Shell Particles using Multistep Ultrasonic Spray Pyrolysis. *Mater. Res. Bull.* **2013**, *48*, 3633–3635. [CrossRef]
33. Jokanovic, V.; Spasic, A.M.; Uskokovic, D. Designing of nanostructured hollow TiO2 spheres obtained by ultrasonic spray pyrolysis. *J. Colloid Interface Sci.* **2004**, *278*, 342–352. [CrossRef]
34. Emil, E.; Alkan, G.; Gurmen, S.; Rudolf, R.; Jenko, D.; Friedrich, B. Tuning the Morphology of ZnO Nanostructures with the Ultrasonic Spray Pyrolysis Process. *Metals* **2018**, *8*, 569. [CrossRef]
35. Çakmak, T.; Kaya, E.E.; Küçük, D.; Ebin, B.; Balci, O.; Gürmen, S. Novel Strategy for One-Step Production of Attenuated Ag-Containing AgCu/ZnO Antibacterial-Antifungal Nanocomposite Particles. *Powder Metall. Met. Ceram.* **2020**, *59*, 261–270. [CrossRef]
36. Stopic, S.; Dvorak, P.; Friedrich, B. Synthesis of nanopowder of copper by ultrasonic spray pyrolysis method. *World Metall. Erzmetall* **2005**, *58*, 191–197.
37. Stopic, S.; Friedrich, B.; Dvorak, P. Synthesis of nanosized spherical silver powder by ultrasonic spray pyrolysis. *Metall* **2006**, *60*, 377–382.
38. Jankovic, B.; Stopic, S.; Bogovic, J.; Friedrich, B. Kinetic and thermodynamic investigations of non-isothermal decomposition process of a commercial silver nitrate in argon atmosphere used as the precursors for ultrasonic spray pyrolysis USP. *Chem. Eng. Process.* **2014**, *82*, 71–87. [CrossRef]
39. Bogovic, J.; Schwinger, A.; Stopic, S.; Schroeder, J.; Gaukel, V.; Schuhmann, P.; Friedrich, B. Controlled droplet size distribution in ultrasonic spray pyrolysis. *Metallurgica* **2011**, *10*, 455–459.
40. Emil Kaya, E.; Kaya, O.; Alkan, G.; Gürmen, S.; Stopic, S.; Friedrich, B. New Proposal for Size and Size-Distribution Evaluation of Nanoparticles Synthesized via Ultrasonic Spray Pyrolysis Using Search Algorithm Based on Image-Processing Technique. *Materials* **2020**, *13*, 38. [CrossRef] [PubMed]